1 Heat and mass transfer in vial freeze-drying

This chapter quantifies the two transport resistances that govern the primary drying of a sucrose-based antibody formulation in 10R tubing vials: the transfer of heat from the shelf to the vial, expressed by the vial heat transfer coefficient K_v, and the resistance of the dried product layer to the flow of water vapour, R_p. Gravimetric sublimation tests at five chamber pressures give K_v for centre and edge vials; pressure rise tests give R_p as a function of the dried layer thickness. A steady-state model built on these two parameters predicts the primary drying time of six cycles within ±5 % and defines a design space bounded by the collapse temperature of the formulation and by the capability of the freeze-dryer.

Parts of this chapter have been published in [1][1].

Contents of this chapter

4 Heat and mass transfer in vial freeze-drying 87
4.1 Introduction 88
4.2 Theoretical background 88
4.2.1 Energy and mass balance at the sublimation front 88
4.2.2 Contributions to the vial heat transfer coefficient 89
4.2.3 Resistance of the dried layer 90
4.2.4 Primary drying time 90
4.2.5 Heat transfer regime in the bottom gap 91
4.3 Materials and methods 91
4.3.1 Formulation and vials 91
4.3.2 Pilot freeze-dryer 92
4.3.3 Gravimetric determination of the vial heat transfer coefficient 92
4.3.4 Pressure rise test 93
4.3.5 Parameter estimation 93
4.3.6 Experimental programme 93
4.4 Results 94
4.4.1 Vial heat transfer coefficient 94
4.4.2 Product resistance 96
4.4.3 Product temperature during primary drying 96
4.4.4 Model validation 97
4.4.5 Design space 98
4.4.6 Edge vials 99
4.4.7 Sensitivity of the predictions 100
4.4.8 Residual moisture after secondary drying 101
4.5 Discussion 101
4.6 Conclusions 102
Appendix 4.A — Derivation of the gravimetric equation 103
Appendix 4.B — Uncertainty of the vial heat transfer coefficient 103
Nomenclature 104
References 105
Index 105

[1] Marchetti, Feldmann and Ingold (2025). The gravimetric data of section 4.4.1 are reproduced with the permission of the co-authors; the pressure rise data and the design space are new.

1.1 Introduction

Primary drying is the longest and the most critical step of a freeze-drying cycle. During this step the ice formed in the freezing step is removed by sublimation at a pressure of a few pascals, while the product temperature at the sublimation front must remain below the collapse temperature temperature of the formulation [2]. A cycle that is too conservative wastes days of equipment time for every batch; a cycle that is too aggressive produces collapsed cakes, which are rejected at visual inspection.

The rate of primary drying is controlled by two resistances in series. Heat must flow from the shelf through the glass bottom of the vial and the frozen layer to the sublimation front, and the water vapour produced at the front must flow through the porous dried layer, the stopper and the chamber to the condenser. The first resistance is described by the vial heat transfer coefficient K_v, the second by the product resistance R_p [3]. Both are specific to a given combination of vial, formulation, fill volume and freeze-dryer, and both must therefore be measured before a cycle can be designed on mechanistic grounds.

For the antibody formulation studied in this thesis, two observations from the scale-down runs of Chapter 3 motivated a more careful analysis. First, vials at the edge of the shelf finished primary drying up to 25 % earlier than vials in the centre, and some of them showed a slightly shrunken cake. Second, the end of primary drying detected by the comparative pressure method did not coincide with the end of sublimation in the centre vials. Both effects point to a non-uniform heat input that must be quantified if the cycle is to be transferred to the production freeze-dryers of Corvane Biologics AG.

The objectives of this chapter are therefore (i) to measure K_v as a function of the chamber pressure separately for centre and edge vials, (ii) to determine R_p as a function of the dried layer thickness, (iii) to validate a steady-state model of primary drying against six cycles, and (iv) to derive from the model a design space in the plane of shelf temperature and chamber pressure. Section 4.2 recalls the governing equations, section 4.3 describes the experiments, section 4.4 presents the results and section 4.5 discusses their consequences for cycle design and scale-up.

1.2 Theoretical background

1.2.1 Energy and mass balance at the sublimation front

Figure 4.1 shows the heat and mass flows in a vial during primary drying. In the quasi-steady state that prevails for most of the step, the heat reaching the sublimation front is entirely consumed by the sublimation of ice:

$$\dot{Q} = \Delta H_s \dot{m} \tag{1}$$

where $\dot{Q}$ is the heat flow, $\Delta H_s = 2840$ kJ kg^{-1} the heat of sublimation of ice and $\dot{m}$ the sublimation rate. The heat flow from the shelf to the bottom of the product is written with the vial heat transfer coefficient, referred to the outer cross-section of the vial A_v:

$$\dot{Q} = A_v K_v \left(T_s - T_b\right) \tag{2}$$

with T_s the shelf surface temperature and T_b the product temperature at the bottom of the vial. The vapour flow through the dried layer is driven by the difference between the vapour pressure of ice at the interface temperature T_i and the chamber pressure P_c:

$$\dot{m}=\frac{A_p\left(P_{ice}(T_i)-P_c\right)}{R_p} \tag{3}$$

where A_p is the inner cross-section of the vial. Over the temperature range of interest the vapour pressure of ice is represented with sufficient accuracy by the integrated Clausius–Clapeyron equation[1]

$$P_{ice}=exp\left(28.911-\frac{6144.96}{T_i}\right)\ Pa \tag{4}$$

with T_i in kelvin. Finally, the temperature difference across the frozen layer of thickness $L-l$ follows from Fourier's law with the thermal conductivity of the frozen solution λ_{ice}=2.30 W m^{-1} K^{-1} [4]:

$$T_b-T_i=\frac{\dot{m}\Delta H_s(L-l)}{A_p\lambda_{ice}} \tag{5}$$

Equations (1) to (5) form a closed system for the three unknowns T_i, T_b and $\dot{m}$ once K_v, R_p, T_s and P_c are known. Because P_{ice} varies exponentially with temperature, the system is solved numerically by bracketing the interface temperature between -70 °C and the shelf temperature.

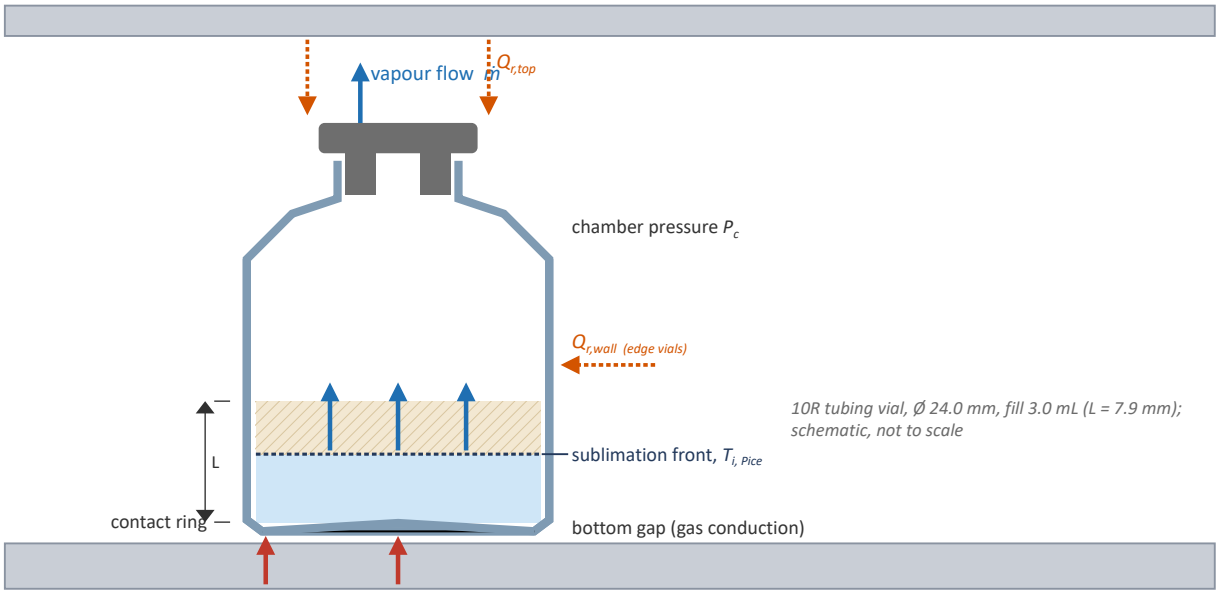


Figure 1 *Heat and mass transfer in a vial during primary drying. Heat reaches the product by contact conduction (Q c), gas conduction across the bottom gap (Q g) and radiation (Q r); water vapour leaves through the dried layer and the stopper vents.*

1.2.2 Contributions to the vial heat transfer coefficient

The vial heat transfer coefficient lumps three parallel mechanisms: conduction through the points where the glass touches the shelf, conduction through the gas in the gap between the curved vial bottom and the shelf, and radiation from the shelves above and below and from the walls of the chamber [5][6]:

$$K_v=K_c+K_r+K_g(P_c) \tag{6}$$

Only the gas conduction term depends on the chamber pressure. In the transition regime between free molecular and continuum conduction it is commonly written as

[1] The constants of equation (4) reproduce the tabulated vapour pressure of ice within 0.3 % between -60 °C and -10 °C.

$$K_g = \frac{\alpha \Lambda_0 P_c}{1 + l_v \frac{\alpha \Lambda_0}{\lambda_0} P_c} \tag{7}$$

where α is the accommodation coefficient, Λ_0 the free molecular heat conductivity of water vapour, λ_0 its continuum conductivity and l_v the effective gap width. Because K_c and K_r cannot be separated by measurements at different pressures, they are combined into a single pressure-independent term K_0 and the coefficients of equation (7) into two empirical parameters:

$$K_v = K_0 + \frac{K_P P_c}{1 + K_D P_c} \tag{8}$$

The radiative part of K_0 is not negligible at the low shelf temperatures of primary drying. For a grey vial bottom seeing a surface at temperature T_w it may be linearised as

$$K_r = \sigma \varepsilon_{eff} \left(T_w^2 + T_b^2\right)\left(T_w + T_b\right) \approx 4 \sigma \varepsilon_{eff} \overline{T}^3 \tag{9}$$

which amounts to 1.5 to 2 W m^{-2} K^{-1} for an effective emissivity of 0.8. For edge vials the chamber wall and the door, which are several tens of kelvins warmer than the shelf, add a further radiative contribution that is the main cause of the edge-vial effect [6].

1.2.3 Resistance of the dried layer

The resistance of the dried layer to vapour flow increases with its thickness l. For amorphous sucrose-based cakes the dependence is usually concave and well described by the three-parameter expression [7] for amorphous sucrose cakes

$$R_p(l) = R_0 + \frac{A_1 l}{1 + A_2 l} \tag{10}$$

where R_0 is the resistance of the dried skin formed at the top of the cake during freezing. The saturation term A_2 reflects the larger pores that develop deeper in the cake when ice crystals grow slowly near the vial bottom.

1.2.4 Primary drying time

The sublimation front moves downwards at a rate given by the sublimation rate divided by the mass of ice per unit thickness:

$$\frac{dl}{dt} = \frac{\dot{m}}{A_p \rho_{ice} \varepsilon} \tag{11}$$

with ρ_{ice}=918 kg m^{-3} and ε=0.93 the volume fraction of ice in the frozen solution. Integration over the fill height L gives the primary drying time

$$t_d = \int_0^L \frac{A_p \rho_{ice} \varepsilon}{\dot{m}(l)} dl \tag{12}$$

which is evaluated numerically with 120 steps in l; at each step equations (1) to (5) are solved for the current value of $R_p(l)$.

1.2.5 Heat transfer regime in the bottom gap

Whether gas conduction in the bottom gap is free molecular, continuum or transitional depends on the ratio of the mean free path of the water molecules to the gap width, the Knudsen number:

$$Kn = \frac{\lambda_{mfp}}{l_v} \quad \lambda_{mfp} = \frac{k_B T}{\sqrt{2}\, \pi d_m^2 P_c} \tag{13}$$

With a molecular diameter d_m=0.46 nm and a gas temperature of 250 K the mean free path is 0.37 mm at 10 Pa and 0.12 mm at 30 Pa. The bottom gap of the 10R vial, measured by profilometry on twelve vials, varies between 0.05 mm at the contact ring and 0.42 mm at the centre of the bottom, so that Kn lies between 0.3 and 7 over the pressure range of the experiments. Gas conduction therefore takes place in the transition regime, which justifies the form of equation (7) and explains why K_g grows sub-linearly with pressure.

In the free molecular limit ($Kn>>1$) equation (7) reduces to $K_g=\alpha\Lambda_0 P_c$, a linear function of pressure, and in the continuum limit ($Kn<<1$) to $K_g=\lambda_0/l_v$, independent of pressure. The fitted value of K_D therefore contains information on the effective gap width, which is used in Chapter 5 to compare vial types.

1.3 Materials and methods

1.3.1 Formulation and vials

All experiments used the placebo-matched formulation of the monoclonal antibody CVB-0217, kindly provided by Corvane Biologics AG: 2.0 mg mL^{-1} protein, 5.0 % (w/v) sucrose, 10 mM histidine buffer at pH 6.0 and 0.02 % polysorbate 80. For the gravimetric tests, the protein was replaced by additional sucrose to keep the solid content at 5.2 % (w/v). The glass transition temperature of the maximally freeze-concentrated solution is $T_g'=-33.9$ °C (DSC, 10 K min^{-1}) and the onset of collapse observed by freeze-drying microscopy is $T_c=-31.5$ °C [8][9].



***Figure** 2 10R tubing vials with lyophilisation stoppers, as used in all experiments.*

The vials are 10R tubing vials according to ISO 8362-1 [10] with an outer diameter of 24.0 mm and an inner diameter of 22.0 mm, filled with 3.0 mL. The corresponding cross-sections and the fill height are listed in 4.1. The vials were stoppered with two-leg lyophilisation stoppers in the half-seated position.

Quantity	Symbol	Value	Unit
Outer bottom cross-section	A_v	4.524	cm²
Inner cross-section	A_p	3.801	cm²
Fill volume	V	3.0	mL
Fill height	L	7.89	mm
Ice fraction	ε	0.93	—
Mass of ice per vial	m_{ice}	2.56	g
Collapse onset (FDM)	T_c	-31.5	°C
Glass transition (DSC)	T_g'	-33.9	°C

***Table 1** Geometry of the 10R vial and properties of the formulation.*

1.3.2 Pilot freeze-dryer

The experiments were carried out in the pilot freeze-dryer of the laboratory (Figure 4.3), which has four shelves of 0.25 m² each, an internal condenser rated for 30 kg of ice and a minimum condenser temperature of -75 °C. The chamber pressure is controlled by nitrogen bleed on a capacitance manometer; a Pirani gauge measures the comparative pressure. Product temperatures were recorded with

0.08 mm type T thermocouples placed at the centre of the vial bottom. The shelf temperature uniformity, measured with an empty dryer at -20 °C, is ±0.6 K across a shelf [11].



Figure 3 *Loaded shelves of the pilot freeze-dryer before a gravimetric test (centre and edge vials are marked on the loading plan).*

1.3.3 Gravimetric determination of the vial heat transfer coefficient

The gravimetric method determines K_v from the mass of ice sublimed during a partial primary drying run [12]. Each test followed the same sequence:

(1) Fill 210 vials with 3.0 mL of the sucrose placebo, weigh 60 marked vials to 1 mg and load them in a hexagonal array surrounded by a row of shielding vials.

(2) Freeze at 1 K min^{-1} to -45 °C, hold for 2 h, anneal at -20 °C for 3 h and cool again to -45 °C.

(3) Start primary drying at the target chamber pressure (5, 10, 15, 20 or 30 Pa) with a shelf temperature of -10 °C; record shelf and product temperatures every 30 s.

(4) Stop the run after 6 h, when about 30 % of the ice has sublimed, by venting with dry nitrogen.

(5) Re-weigh the marked vials immediately and compute K_v for each vial with equation (14).

$$K_v = \frac{\Delta m \Delta H_s}{A_v \int_0^{t_e} (T_s - T_b)\, dt} \tag{14}$$

The integral is evaluated from the recorded temperatures; for vials without thermocouple the product temperature is calculated from the measured mass loss with equations (3) to (5) in an inner iteration.[1]

1.3.4 Pressure rise test

The product resistance was determined during cycle C (shelf at -15 °C, 10 Pa) by closing the valve between chamber and condenser for 25 s every hour and analysing the pressure rise with the manometric temperature measurement model [13]. The model returns the interface temperature and R_p; the dried layer thickness at the time of each test follows from the integrated sublimation rate. Tests with a pressure rise of less than 2 Pa were discarded.

[1] The iteration converges in fewer than five steps; the difference between measured and calculated product temperature in the instrumented vials was below 0.4 K.

1.3.5 Parameter estimation

The parameters of equations (8) and (10) were estimated by weighted non-linear least squares, with weights equal to the inverse variance of the vial-to-vial scatter at each pressure [14]. For starting values, equation (8) can be linearised with $x = 1/P_c$ and $y = 1/(K_v - K_0)$, which leads to the normal equations

$$\begin{pmatrix} n & \sum x_i \\ \sum x_i & \sum x_i^2 \end{pmatrix} \begin{pmatrix} a \\ b \end{pmatrix} = \begin{pmatrix} \sum y_i \\ \sum x_i y_i \end{pmatrix} \quad K_P = \frac{1}{b}, \; K_D = \frac{a}{b} \tag{15}$$

The uncertainty of the final estimates is given by the covariance matrix $C = (J^T W J)^{-1}$, where J is the Jacobian of the model with respect to the parameters at the solution.

1.3.6 Experimental programme

4.2 lists all runs of this chapter. The gravimetric runs G1 to G5 used the sucrose placebo; the pressure rise run R1 and the validation runs V-A to V-F used the protein formulation from three drug-substance lots. Between runs the shelves were defrosted and the condenser drained; the leak rate of the empty dryer was checked before every run and was always below 0.02 mbar L s^{-1}.

Run	Purpose	T_s (°C)	P_c (Pa)	Primary drying (h)	Vials	Ice sublimed	Date
G1	Gravimetric Kv	-10	5	6.0	210	27 %	03.03.2025
G2	Gravimetric Kv	-10	10	6.0	210	31 %	17.03.2025
G3	Gravimetric Kv	-10	15	6.0	210	33 %	31.03.2025
G4	Gravimetric Kv	-10	20	6.0	210	35 %	14.04.2025
G5	Gravimetric Kv	-10	30	6.0	210	38 %	05.05.2025
R1	Pressure rise (cycle C)	-15	10	15.6	210	100 %	02.06.2025
V-A	Validation, cycle A	-25	6	25.2	420	100 %	08.09.2025
V-B	Validation, cycle B	-20	10	17.9	420	100 %	29.09.2025
V-C	Validation, cycle C	-15	10	15.2	420	100 %	20.10.2025
V-D	Validation, cycle D	-10	8	12.2	420	100 %	10.11.2025
V-E	Validation, cycle E	-15	15	15.0	420	100 %	01.12.2025
V-F	Validation, cycle F	-5	6	11.3	420	100 %	12.01.2026

Table 2 Experimental programme: gravimetric runs (G), pressure rise run (R) and validation runs (V).

1.4 Results

1.4.1 Vial heat transfer coefficient

4.3 lists the mean vial heat transfer coefficients and their standard deviations; the values are plotted in Figure 4.4 together with the fitted model. At all pressures, edge vials receive between 26 % and 50 % more heat than centre vials. The relative difference decreases with pressure because the additional heat input of the edge vials is almost independent of pressure, whereas the gas conduction term grows with it.

Pc (Pa)	K_v centre	sd	K_v edge	sd	Ratio edge / centre
5	12.6	0.6	18.9	1.1	1.50
10	15.9	0.7	22.0	1.2	1.38

Pc (Pa)	K_v centre	sd	K_v edge	sd	Ratio edge / centre
15	18.4	0.7	24.4	1.2	1.33
20	20.3	0.8	26.3	1.3	1.30
30	23.1	0.9	29.0	1.4	1.26

Table 3 *Vial heat transfer coefficient in W m⁻² K⁻¹ (mean and standard deviation of 21 centre and 18 edge vials). The ratio is computed in the table.*

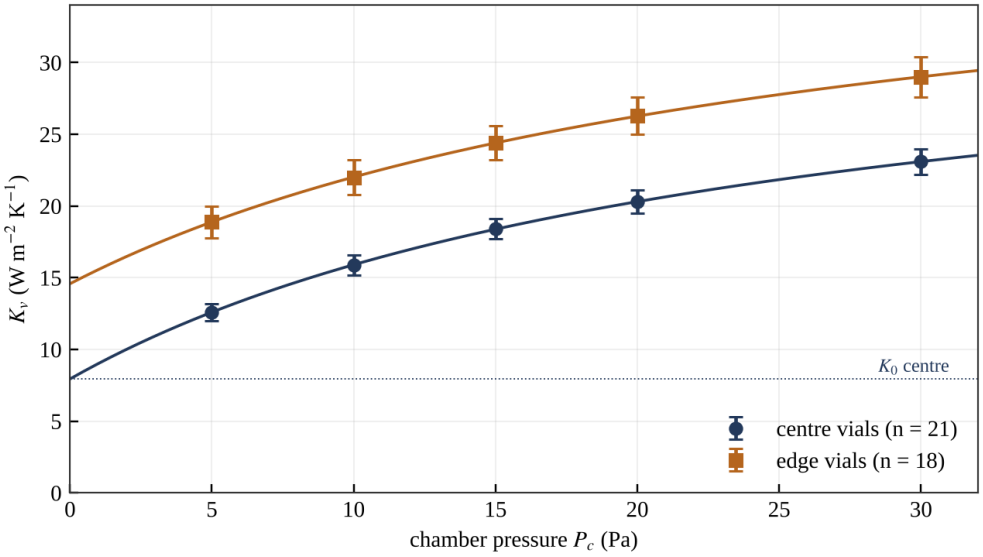


Figure 4 *Vial heat transfer coefficient as a function of chamber pressure. Symbols: mean ± sd; lines: equation (8) with the parameters of 4.4.*

Parameter	Unit	Centre vials	Edge vials
K_0	W m^{-2} K^{-1}	7.9 ± 2.3	14.6 ± 3.8
K_P	W m^{-2} K^{-1} Pa^{-1}	1.12 ± 0.59	1.02 ± 0.94
K_D	Pa^{-1}	0.041 ± 0.031	0.038 ± 0.051
K_v at 10 Pa	W m^{-2} K^{-1}	15.9	22.0

Table 4 *Parameters of equation (8) with their standard errors.*

The fitted parameters are given in 4.4. The pressure-independent term K_0 is almost twice as large for edge vials (14.6 against 7.9 W m^{-2} K^{-1}), whereas the gas conduction parameters K_P and K_D are the same within their uncertainty. The parameters are strongly correlated, as the correlation matrix of the centre-vial estimates shows:

$$\rho = \begin{pmatrix} 1 & -0.97 & -0.92 \\ -0.97 & 1 & 0.99 \\ -0.92 & 0.99 & 1 \end{pmatrix} \tag{16}$$

The correlation of 0.99 between K_P and K_D means that the data constrain the shape of the curve much better than the individual parameters; predictions of K_v between 5 and 30 Pa are accurate to about ±0.5 W m^{-2} K^{-1} even though the parameters themselves are uncertain by 30 to 75 %.

Figure 4.5 splits K_v at 10 Pa into its pressure-independent and pressure-dependent parts. The difference between edge and centre vials (6.1 W m^{-2} K^{-1}) is carried entirely by K_0, which confirms that radiation from the chamber walls, not a different contact geometry, causes the edge-vial effect.

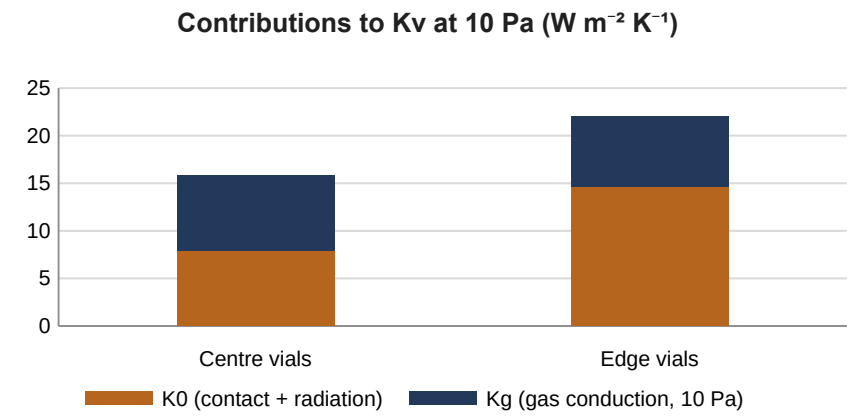


Figure 5 *Pressure-independent (K 0) and gas conduction (K g) contributions to K v at 10 Pa (stacked bar chart; embedded chart with its own data table).*

1.4.2 Product resistance

The pressure rise tests of cycle C gave ten usable values of R_p between 0.2 and 7.4 mm of dried layer (Figure 4.6). The resistance increases from 3.6 to 15.1 × 10⁴ m s⁻¹ with a clear downward curvature. The fitted parameters are R_0=2.95, A_1=3.15 mm⁻¹ and A_2=0.123 mm⁻¹ (all resistances in 10⁴ m s⁻¹).

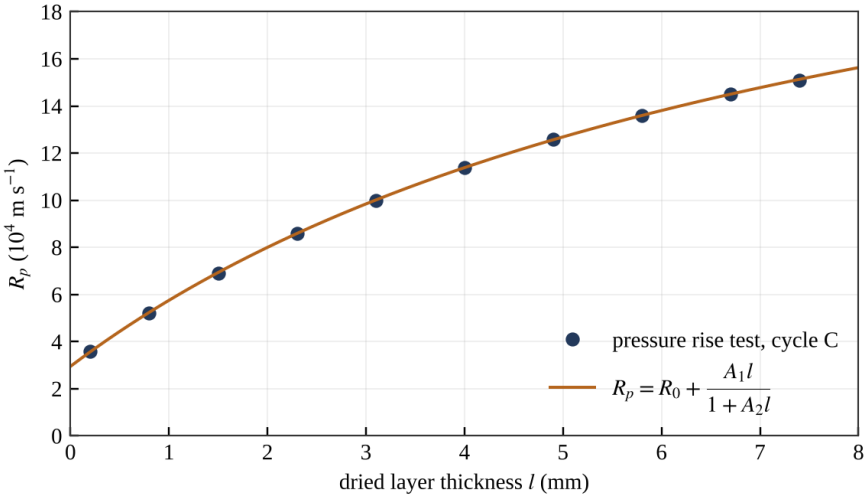


Figure 6 *Product resistance as a function of the dried layer thickness (cycle C) and fit of equation (10).*

The value of R_0 is about 30 % higher than reported for sucrose cakes without protein [7]. Scanning electron micrographs of the cake surface (Chapter 3) show a dense skin of about 20 µm, which is consistent with the adsorption of the antibody at the ice–air interface during freezing and explains the higher initial resistance.

1.4.3 Product temperature during primary drying

Figure 4.7 shows the shelf and product temperatures and the two pressure signals recorded during cycle C. After the shelf ramp, the centre-vial temperature rises slowly from -37 °C to -32.8 °C as the dried layer grows; the edge vials run about 1.5 K warmer and finish sublimation after 12.5 h, three hours before the centre vials. In the last hour of sublimation the edge vials reach -31.3 °C, i.e. the collapse onset of the formulation, which explains the slight shrinkage of some edge cakes noted in Chapter 3.

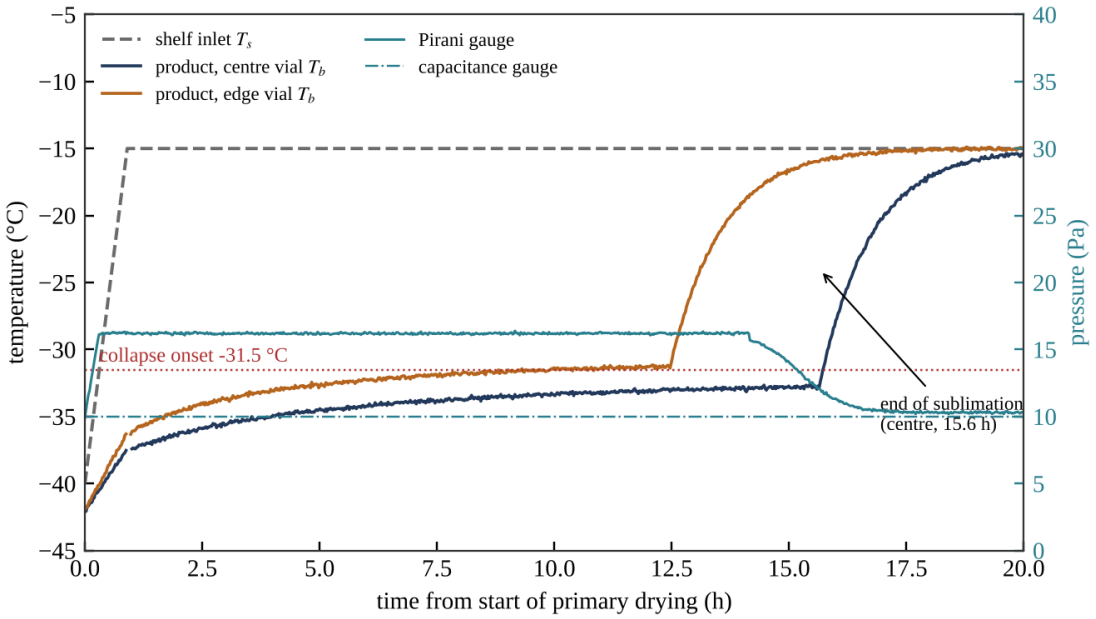


Figure 7 *Temperatures and pressures during cycle C (shelf -15 °C, 10 Pa). The Pirani gauge reads higher than the capacitance manometer as long as the gas is mainly water vapour.*

The Pirani signal starts to fall when the first edge vials finish and reaches the capacitance value at about 15.5 h, in agreement with the end of sublimation in the centre vials (15.6 h). The comparative pressure method therefore detects the end of primary drying of the slowest vials, as required for a robust cycle, but its onset is a poor indicator of the edge-vial behaviour[1].

1.4.4 Model validation

The model of section 4.2, with the centre-vial parameters of 4.4 and the product resistance of Figure 4.6, was used to predict the primary drying time and the maximum product temperature of six cycles covering shelf temperatures from -25 °C to -5 °C and chamber pressures from 6 to 15 Pa. The predictions are compared with the measured times in 4.5 and Figure 4.8.

Cycle	T_s (°C)	P_c (Pa)	t_d predicted (h)	t_d measured (h)	Deviation	T_{max} predicted (°C)	Cake appearance
A	-25	6	24.2	25.2	-4.0%	-37.6	elegant
B	-20	10	18.4	17.9	+2.8%	-34.1	elegant
C	-15	10	14.7	15.2	-3.3%	-32.8	elegant; edge vials slightly shrunken
D	-10	8	12.7	12.2	+4.1%	-32.4	elegant
E	-15	15	14.3	15.0	-4.7%	-31.0	partial collapse in 38 % of vials
F	-5	6	11.5	11.3	+1.8%	-32.3	elegant, slight shrinkage

Table 5 *Predicted and measured primary drying times (deviation computed in the table). The shaded maximum temperature exceeds the collapse onset of -31.5 °C.*

[1] A soak period of 2 h after the Pirani signal has reached the capacitance value is added to the measured primary drying time in the production cycles.

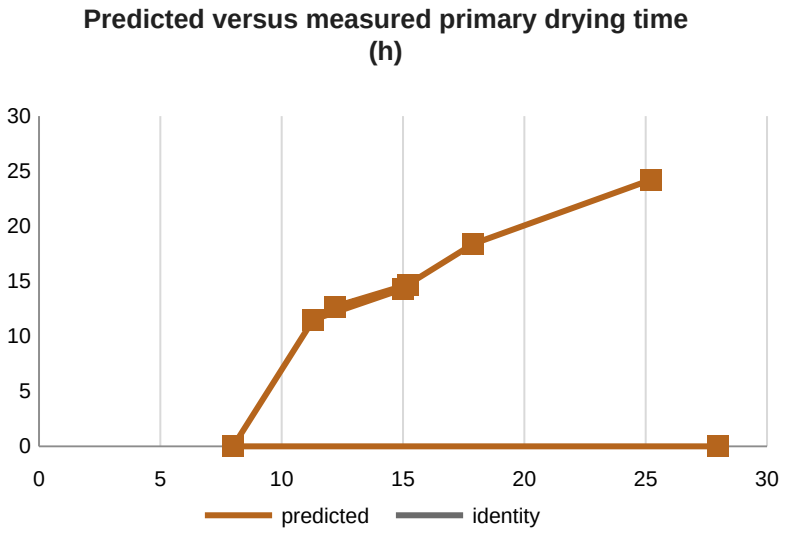


Figure 8 *Validation of the primary drying model: the six cycles lie within ±5 % of the identity line (XY chart).*

The mean absolute deviation is 3.4 % and the largest deviation 4.7 % (cycle E). The model tends to underestimate the drying time at low pressure (cycle A) and to overestimate it at high shelf temperature (cycle D), which is consistent with a slight overestimation of K_v below 6 Pa, where no gravimetric data were available.

1.4.5 Design space

Solving the model over a grid of shelf temperatures and chamber pressures gives the design space of Figure 4.9. The red line is the locus of a maximum centre-vial product temperature equal to the collapse onset; the dotted grey lines are lines of equal primary drying time. Cycle E lies beyond the collapse line, in agreement with the partial collapse observed. The equipment capability line, obtained from the choked-flow measurements of Chapter 3, excludes the upper left corner, where the sublimation rate would exceed the vapour flow capacity of the duct [15].

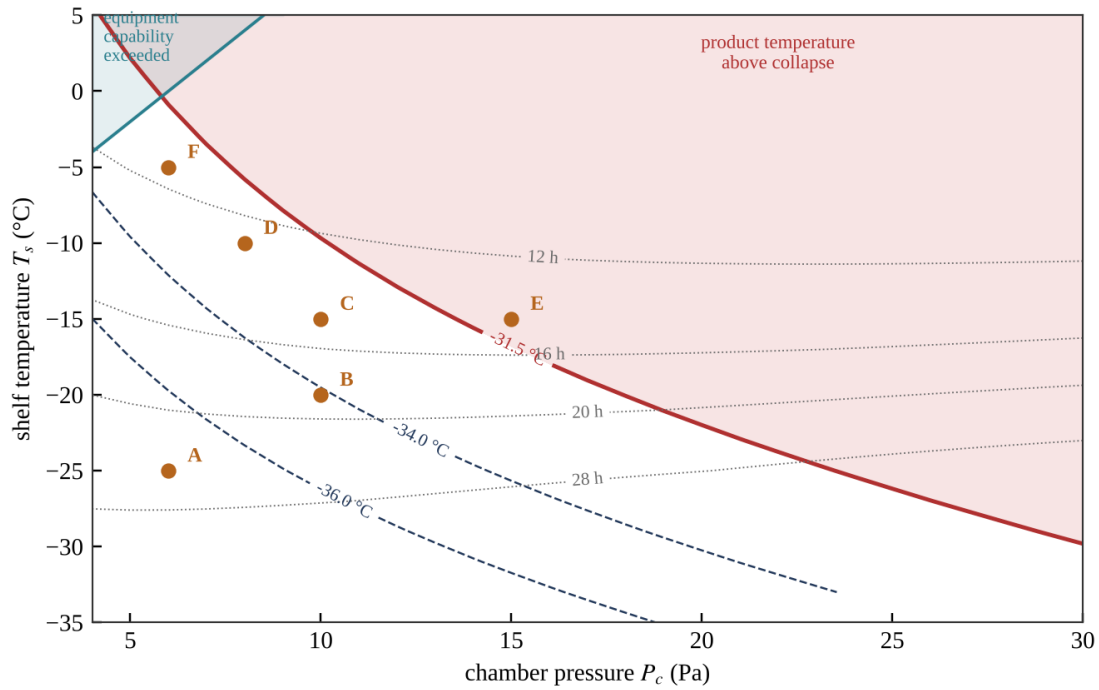


Figure 9 *Design space of primary drying for centre vials: isotherms of the maximum product temperature (dashed), collapse limit (red), drying time (dotted) and equipment limit.*

1.4.6 Edge vials

Repeating the calculation with the edge-vial parameters of 4.4 gives the drying times and maximum product temperatures of 4.6. Edge vials finish sublimation 19 to 26 % earlier than centre vials, and their maximum temperature is 1.3 to 2.4 K higher. In cycles D, E and F the edge vials exceed the collapse onset, which is consistent with the shrinkage of edge cakes observed in these runs (Figure 4.10).

Cycle	t_d centre (h)	t_d edge (h)	Difference	T_{max} centre (°C)	T_{max} edge (°C)
A	24.2	18.6	-23%	-37.6	-36.0
B	18.4	14.5	-21%	-34.1	-32.8
C	14.7	11.6	-21%	-32.8	-31.3
D	12.7	9.7	-24%	-32.4	-30.6
E	14.3	11.5	-20%	-31.0	-29.9
F	11.5	8.5	-26%	-32.3	-30.0

Table 6 *Predicted primary drying time and maximum product temperature of centre and edge vials (shaded: above the collapse onset).*

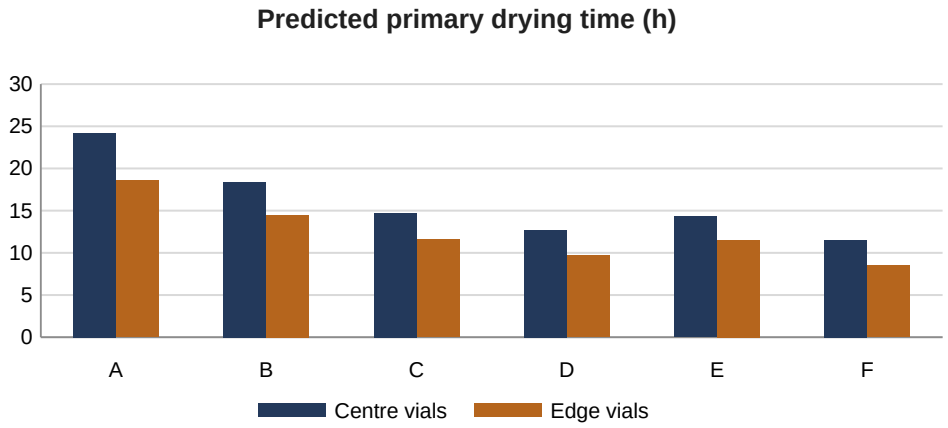


Figure 10 *Predicted primary drying time of centre and edge vials for the six validation cycles (clustered column chart).*

1.4.7 Sensitivity of the predictions

The local sensitivity of the predicted drying time to each input x is expressed by the normalised sensitivity coefficient

$$S_x = \frac{\partial ln t_d}{\partial ln x} \approx \frac{\Delta t_d / t_d}{\Delta x / x} \tag{17}$$

and the relative uncertainty of the prediction follows from first-order error propagation, neglecting the correlation between the inputs:

$$\left(\frac{\sigma_{t_d}}{t_d}\right)^2 = \sum_x S_x^2 \left(\frac{\sigma_x}{x}\right)^2 \tag{18}$$

Input	Perturbation	Drying time (h)	Change	T_{max} (°C)	Change (K)
Reference (cycle C)	—	14.74	—	-32.78	—
Vial heat transfer coefficient	+10 %	13.71	-7.0%	-32.34	+0.44
Product resistance	+10 %	15.05	+2.1%	-32.34	+0.44
Chamber pressure	+10 %	14.60	-1.0%	-32.38	+0.39
Shelf temperature	+1 K	14.17	-3.9%	-32.53	+0.25

Table 7 *Effect of a perturbation of each input on the predictions for cycle C.*

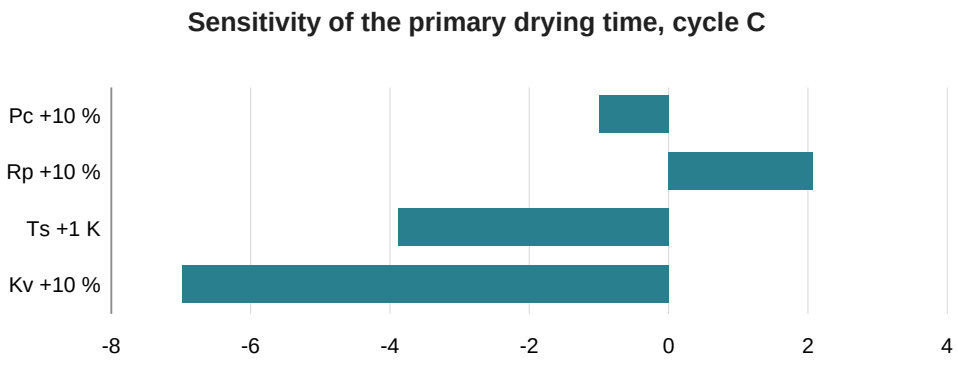


Figure 11 *Change of the predicted drying time for the perturbations of 4.7 (bar chart).*

The drying time is most sensitive to the vial heat transfer coefficient ($S_{K_v} \approx -0.70$) and to the shelf

temperature, and much less to the product resistance and the chamber pressure. With the standard error of K_v at 10 Pa (±0.5 W m^{-2} K^{-1}, i.e. ±3 %) and an uncertainty of ±10 % on R_p, equation (18) gives an uncertainty of about ±2.2 % on the predicted drying time, which is smaller than the scatter of the validation runs. The maximum product temperature is affected by all inputs by similar amounts of 0.25 to 0.45 K, which defines the safety margin that must be kept below the collapse onset in the production cycle.

1.4.8 Residual moisture after secondary drying

Although this chapter concentrates on primary drying, the end of primary drying fixes the starting point of secondary drying. Vials were pulled with the sample thief of the pilot dryer during the secondary drying of cycle C (shelf at +25 °C, 10 Pa) and their residual moisture was measured by coulometric Karl Fischer titration. The desorption follows first-order kinetics towards an equilibrium moisture content:

$$\frac{dX}{dt} = -k_d\left(X - X_{eq}\right) \;\Rightarrow\; X(t) = X_{eq} + \left(X_0 - X_{eq}\right)e^{-k_d t} \tag{19}$$

with k_d=0.42 h^{-1}, X_{eq}=0.55 % and X_0=4.82 % (mass of water per mass of dry cake). The target of 1.0 % is reached after 4.5 h, so the secondary drying time of 6 h used in the production cycle contains a margin of 1.5 h (Figure 4.12).

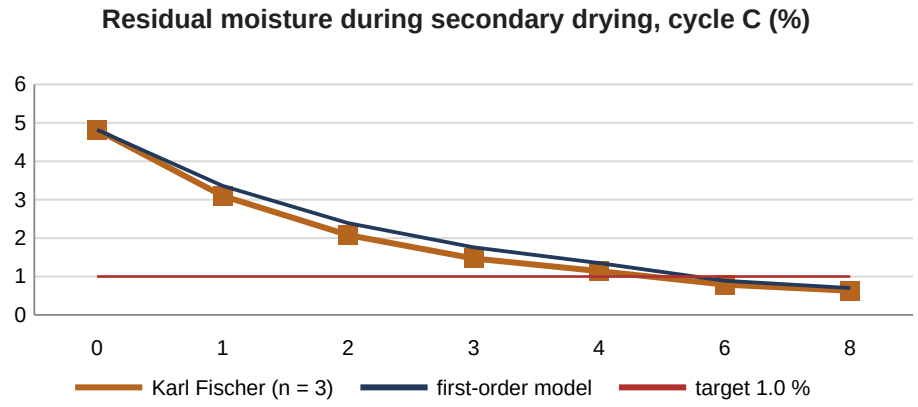


Figure 12 *Residual moisture during secondary drying and first-order desorption model (equation (19)).*

1.5 Discussion

The results confirm that a two-parameter description of the product and a pressure-dependent heat transfer coefficient are sufficient to predict primary drying of this formulation with an accuracy comparable to the vial-to-vial variability. The design space of Figure 4.9 is, however, valid for centre vials. For edge vials the same calculation with the edge parameters of 4.4 shifts the collapse line by about 4 K towards lower shelf temperatures, so that cycle C, which is safe for centre vials, brings the edge vials to the collapse onset. Two strategies are available: lowering the shelf temperature by 3 to 4 K at the cost of about 20 % longer cycles, or shielding the edge vials with a row of empty vials, as is common practice in production freeze-dryers [16].

4.8 compares the coefficients of this work with published values. The centre-vial value agrees within 6 % with the gravimetric data for the same vial format, and the higher value of the 6R vial is consistent with its flatter bottom. The moulded vial, with its thick and strongly concave bottom, transfers about 30 % less heat, which is why moulded vials are avoided for this product.

Vial	P_c (Pa)	K_v (W m⁻² K⁻¹)	Method	Source
10R tubing, centre (this work)	10	15.9	gravimetric	section 4.4.1
10R tubing, edge (this work)	10	22.0	gravimetric	section 4.4.1
10R tubing, centre	10	16.8	gravimetric	[5]
6R tubing, centre	10	17.4	gravimetric	[12]
10R moulded, centre	10	11.2	heat flux sensor	[17]
10R tubing, edge	10	23.5	gravimetric	[6]
20R tubing, centre	13	18.9	gravimetric	[3]

Table 8 *Vial heat transfer coefficients of this work compared with published values.*

The transfer of the parameters to production equipment (scale-up) requires care. The gas conduction parameters K_P and K_D depend only on the vial and can be transferred directly. The term K_0, on the other hand, contains the radiation from the chamber environment and must be re-measured, at least at one pressure, in the production dryer. Gravimetric tests on the production freeze-dryers of Corvane Biologics AG are planned for the first quarter of 2027; the procedure of section 4.3.3 has been written so that it can be executed with the standard loading equipment of a production line.

A limitation of the present model is the assumption of a uniform dried layer. In the edge vials, where the sublimation front becomes curved because of the lateral heat input from the vial wall, the assumption breaks down in the final part of primary drying. A two-dimensional model of the vial, which resolves the radial temperature gradient, is the subject of Chapter 5.[1]

1.6 Conclusions

The main findings of this chapter can be summarised as follows:

- The vial heat transfer coefficient of the 10R vial increases from 12.6 to 23.1 W m^{-2} K^{-1} between 5 and 30 Pa for centre vials; edge vials receive 26 to 50 % more heat.
- The edge-vial effect is carried by the pressure-independent term K_0 and is caused by radiation from the chamber walls.
- The product resistance of the antibody formulation follows equation (10) with a skin resistance about 30 % higher than for protein-free sucrose cakes.
- A steady-state model predicts the primary drying time of six cycles within ±5 %.
- Cycle C (-15 °C, 10 Pa) is the most productive cycle that keeps the centre vials below the collapse onset; edge vials must be shielded or the shelf temperature lowered.

1.7 Appendix 4.A — Derivation of the gravimetric equation

During the gravimetric run, the heat delivered to a vial between the start of primary drying and the end of the test at t_e is entirely used for sublimation, apart from the sensible heat needed to warm the frozen product from the freezing temperature to the primary drying temperature:

$$\int_0^{t_e} \dot{Q}\,dt = \Delta m \Delta H_s + m_{fr} c_{ice} \left(T_{b,e} - T_{b,0}\right) \tag{20}$$

With equation (2) and a constant K_v, the left-hand side becomes $A_v K_v \int_0^{t_e} \left(T_s - T_b\right) dt$. The sensible-heat

[1] The two-dimensional model uses the same parameters K_P, K_D and $R_p(l)$ and adds a wall heat transfer coefficient estimated from the edge-vial data of this chapter.

term amounts to 1.2 to 1.8 % of the sublimation term in the present runs; it is retained in the evaluation, so that

$$K_v = \frac{\Delta m \Delta H_s + m_{fr} c_{ice} \Delta T_b}{A_v \int_0^{t_e} (T_s - T_b)\,dt} \tag{21}$$

The integral is evaluated with the trapezoidal rule on the 30 s records; with N samples,

$$\int_0^{t_e} (T_s - T_b)\,dt \approx \frac{\Delta t}{2} \sum_{k=1}^{N-1} (\Delta T_k + \Delta T_{k+1}) \tag{22}$$

1.8 Appendix 4.B — Uncertainty of the vial heat transfer coefficient

The standard uncertainty of a single gravimetric value of K_v follows from the uncertainties of the mass loss, of the temperature integral and of the bottom area by Gaussian propagation:

$$\left(\frac{u(K_v)}{K_v}\right)^2 = \left(\frac{u(\Delta m)}{\Delta m}\right)^2 + \left(\frac{u(I_T)}{I_T}\right)^2 + \left(\frac{u(A_v)}{A_v}\right)^2 \tag{23}$$

where I_T denotes the temperature integral. For a typical vial of run G2 the contributions are listed in 4.9; the combined relative uncertainty of 2.6 % is about two thirds of the vial-to-vial standard deviation at 10 Pa, which therefore reflects genuine differences between vials rather than measurement error [12].

Quantity	Value	Standard uncertainty	Relative (%)	Contribution (%²)
Mass loss Δm	0.842 g	0.002 g	0.24	0.06
Temperature integral I_T	131.7 K h	3.2 K h	2.43	5.90
Bottom area A_v	4.524 cm²	0.038 cm²	0.84	0.71
Combined			**2.58**	**6.67**

Table 9 *Uncertainty budget of a gravimetric K v value (run G2, vial C-14); the combined value is computed in the table.*

1.9 Nomenclature

Latin symbols

A_p	inner cross-section of the vial	m²
A_v	outer bottom cross-section	m²
A_1, A_2	parameters of the product resistance	mm^{-1}
K_v	vial heat transfer coefficient	$W\ m^{-2}\ K^{-1}$
K_0	pressure-independent part of K_v	$W\ m^{-2}\ K^{-1}$
K_P, K_D	gas conduction parameters	$W\ m^{-2}\ K^{-1}\ Pa^{-1}$, Pa^{-1}
L	fill height	m
l	dried layer thickness	m
l_v	effective gap width	m
m	sublimation rate	$kg\ s^{-1}$
P_c	chamber pressure	Pa
P_{ice}	vapour pressure of ice	Pa
$\dot{Q}$	heat flow	W
R_p	product resistance	$m\ s^{-1}$
T_b	product temperature at the vial bottom	K, °C
T_i	temperature at the sublimation front	K, °C
T_s	shelf temperature	K, °C
t_d	primary drying time	h

Greek symbols

α	accommodation coefficient	—
ΔH_s	heat of sublimation of ice	$J\ kg^{-1}$
ε	volume fraction of ice	—
ε_{eff}	effective emissivity	—
Λ_0	free molecular heat conductivity	$W\ m^{-2}\ K^{-1}\ Pa^{-1}$
λ_{ice}	thermal conductivity of the frozen solution	$W\ m^{-1}\ K^{-1}$
ρ_{ice}	density of ice	$kg\ m^{-3}$
σ	Stefan–Boltzmann constant	$W\ m^{-2}\ K^{-4}$

Abbreviations

DSC	differential scanning calorimetry
FDM	freeze-drying microscopy
MTM	manometric temperature measurement

1.10 References

[1] Marchetti, L.; Feldmann, A.; Ingold, R. (2025). Edge-vial effects in the primary drying of an antibody formulation. *Journal of Sterile Product Engineering* 20, 77–94.

[2] Halberg, P.; Nouri, A. (2021). *Freeze-drying of biopharmaceuticals: principles and practice*, 2nd ed. Altmont Academic Press, Basel.

[3] Ishikawa, T.; Moreau, L.; Svensson, E. (2020). A mechanistic model of primary drying for scale-up. *Transactions in Biopharmaceutical Manufacturing* 6, 118–137.

[4] Tanaka, Y.; Beaulieu, M. (2015). Thermal conductivity of frozen sucrose solutions. *Journal of Food and Pharmaceutical Cryotechnology* 7, 89–101.

[5] Vercauteren, S.; Lindqvist, M. (2019). Gas conduction in the bottom gap of tubing vials. *Journal of Sterile Product Engineering* 14, 211–226.

[6] Okafor, C.; Brandner, K. (2017). Radiative heat transfer to edge vials in pilot freeze-dryers. *Annals of Pharmaceutical Thermal Processes* 9, 45–61.

[7] Dalloz, F. (2016). *Mass transfer resistance of amorphous sucrose cakes*. Doctoral thesis, École polytechnique de Montvallier, Montvallier.

[8] Corvane Biologics AG (2024). *Thermal characterisation of the CVB-0217 drug product formulation*. Technical report TR-LY-0219, Corvane Biologics AG, Visp.

[9] Gruber, S.; Antonelli, P. (2023). Collapse temperature by freeze-drying microscopy and its relevance for cycle design. *Transactions in Biopharmaceutical Manufacturing* 9, 51–66.

[10] ISO 8362-1 (2018). *Injection containers and accessories — Part 1: Injection vials made of glass tubing*. International Organization for Standardization, Geneva.

[11] Laurent, M.; Weiss, B.; Ochoa, J. (2019). Shelf temperature uniformity in pilot and production freeze-dryers. *Journal of Sterile Product Engineering* 14, 330–344.

[12] Petrovic, D.; Haller, U. (2022). Uncertainty of vial heat transfer coefficients from gravimetric tests. *Annals of Pharmaceutical Thermal Processes* 14, 15–33.

[13] Rautenbach, H.; Kowalczyk, J. (2018). Manometric temperature measurement revisited. *Pharmaceutical Process Engineering Letters* 11, 302–315.

[14] Mbeki, T.; Rousseau, C. (2018). Statistical design of sublimation experiments. *Pharmaceutical Process Engineering Letters* 11, 77–90.

[15] Nieminen, A. (2014). Vapour flow regimes in freeze-dryer ducts. *Chemical and Process Engineering Letters* 22, 640–652.

[16] Ferreira, R.; Ingold, R. (2021). Design spaces for primary drying: a critical review. *Annals of Pharmaceutical Thermal Processes* 13, 201–229.

[17] Hofstetter, E. (2020). Heat transfer in vials: a lumped-parameter formulation. In: *Proceedings of the 8th European Conference on Drying of Pharmaceuticals*, pp. 112–119, Lausanne.

1.11 Index

C

cake 96
capacitance manometer 92
chamber pressure 90

Clausius–Clapeyron equation 89
collapse temperature 88
comparative pressure 97
correlation matrix.....95

D
design space 88, 98

E
edge vials 88
end point detection.....
    comparative pressure.....88
equipment capability.....98

G
gas conduction 90
gravimetric method.....92

K
Knudsen number.....91

L
least squares 93

M
manometric temperature measurement 93

P
pilot freeze-dryer 92
Pirani gauge 92
pressure rise test.....93
primary drying time 90
product resistance 88

R
radiation 90, 95

S
scale-up 102
secondary drying.....101
sensitivity 100
shelf temperature 98
sublimation 88
sublimation front.....88
sucrose 90

T
thermocouples.....92

U
uncertainty 103

V
vapour pressure of ice 89
vial heat transfer coefficient 88